Examination of the Shear Stress Transport Assumption with a Low-Reynolds Number $k-\omega$ Model for Aerodynamic Flows

Shia-Hui Peng*† , Peter Eliasson‡
Swedish Defence Research Agency (FOI), SE-164 90 Stockholm, Sweden
Lars Davidson§
Chalmers University of Technology, SE-412 96 Gothenburg, Sweden

Using a low-Reynolds number $k-\omega$ model and its high-Reynolds number variant as base models, the Shear Stress Transport (SST) concept is examined in computations of flows around the RAE2822 airfoil and the DLR-F6 wind-body configuration. Both flows are characterized by local boundary layer separation. Based on an analysis of the *net* production for the turbulent kinetic energy, k, and for its specific dissipation rate, ω, the rationale is highlighted behind the SST formulation that enables improved predictions of flow separation. It is shown that the SST formulation may make the modeling contain the growth of the production of k and, consequently, suppress the turbulent diffusion. Incorporating the SST assumption, the model responds more appropriately to the effect of an adverse pressure gradient in the boundary layer and produces more extended flow separation bubble than the original base model. Improvement due to the SST formulation is also observed in predictions of the shock location for the transonic aerodynamic flows considered in this work.

Nomenclature

c	Chord of wing or airfoil
C_p	Pressure coefficient
C_*	Model constants with different subscript $(_*)$
f_*	Model functions with different subscript $(_*)$
k	Turbulent kinetic energy
M	Mach number
S	Magnitude of flow strain rate tensor, S_{ij}
u	Streamwise (x-direction) velocity component
v	Vertical (y-direction) velocity component
w	Spanwise (z-direction) velocity component
ε	Turbulent dissipation rate of k
μ	Molecular dynamic viscosity of fluid
μ_t	Turbulent eddy viscosity
σ_k	Model constant
σ_ω	Model constant
ω	Specific turbulent dissipation rate
Subscript	
ref	Reference
∞	Freestream

*Research Director, Department of Computational Physics, FOI. Corresponding author (peng@foi.se). AIAA member.
†Adjunct Professor, Department of Applied Mechanics, Chalmers University of Technology.
‡Deputy Research Director, Department of Computational Physics, FOI. AIAA member.
§Professor, Department of Applied Mechanics, Chalmers University of Technology.

I. Introduction

While Computational Fluid Dynamics (CFD) has been commonly used in aeronautic applications, where the dominant flow features are often characterized by large Reynolds number and turbulence, its success relies heavily on the modelling of flow physics. Indeed, turbulence modeling has been frequently underlined in aeronautical applications as one of the major obstacles towards accurate and efficient flow predictions.[1,2] It has been, and will remain in the foreseeable future, an important issue in studies aiming at improving CFD robustness and accuracy. Extensive attention has thus been paid to the development of improved turbulence models, ranging from Reynolds-Averaged Navier-Stokes (RANS) approaches to SubGrid-Scale (SGS) modeling in large eddy simulation (LES).

In industrial CFD applications, RANS modelling remains one of the main approaches when dealing with turbulent flows. Over decades, this has consequently facilitated the development of a great variety of RANS turbulence models. Modelling approaches in the context of RANS have shown different degrees of success in various engineering applications, spanning from mixing-length models, linear and nonlinear eddy viscosity models to algebraic and differential Reynolds stress models with a hierarchy of increasing complexity in the modelling formulation and related CFD implementations. For an appropriate compromise between computational efficiency and accuracy, nonetheless, only a few of RANS models have been popularized in the routine use of aerodynamic CFD applications, one of which is the shear stress transport (SST) model proposed by Menter.[3,4]

Menter's SST model has been built on a baseline model (namely, the BSL model),[3] which combines the Wilcox $k-\omega$ model[5] in the near-wall region with the $k-\varepsilon$ model in the outer part of the boundary layer. For convenient use, the off-wall $k-\varepsilon$ model is transformed into a $k-\omega$ formulation. Adopting the same turbulent transport equations as in the BSL model, the SST model incorporates further the Bradshaw's hypothesis into the formulation for the turbulent eddy viscosity, which assumes that the principal turbulent shear stress is linearly aligned with the turbulent kinetic energy, k. The *SST assumption* is referred here to Menter's eddy-viscosity formulation based on the Bradshaw assumption. The availability of the SST assumption holds reasonably well for boundary layer separation due to adverse pressure gradient. In simulations of separating aerodynamic flows, indeed, the success reached with the SST model may largely be attributed to the SST assumption inherent in the modelling formulation. The baseline (BSL) model, on the other hand, enables an alleviation of freestream sensitivity in the outer edge of the boundary layer due to the combined $k-\varepsilon$ model.

One of the main purposes with the present work is to explore the performance of the SST assumption incorporated into an alternative eddy viscosity model for turbulent aerodynamic flows. A modified $k-\omega$ model, with both a low-Reynolds number (LRN) and a high-Reynolds number (HRN) version, proposed previously by Peng et al.,[6,7] is adopted as the base model. The formulated LRN and HRN SST models are then examined in computations for flows around, respectively, the RAE2822 airfoil and the DLR-F6 wing-body configuration. In the following sections, we describe first the rationale and formulation of SST modelling, the results computed from the test cases are then presented and discussed in comparison with available experimental data. This is followed by a conclusion of the present work.

II. SST Modelling Formulation

The concept of shear stress transport is based on the Bradshaw assumption, which suggests that a linear relation holds in the boundary layer between the principal turbulent shear stress, τ, and the turbulent kinetic energy, viz. $\tau = a_1\rho k$, where a_1 is a constant. Menter has made this assumption adapted to the eddy viscosity formulation in his SST model, which has shown obvious superiority over the standard $k-\omega$ model by Wilcox[5] in predictions of boundary layer flow separation. Pragmatically, the SST assumption can be adapted to, and exploited by, other alternative eddy-viscosity models.

Prior to the presentation of the examined $k-\omega$ model in conjunction with the SST concept, an analysis is provided first to highlight the difference in modelling the turbulence production between the SST formulation and other conventional linear eddy-viscosity models.

A. Rationale on the SST Formulation

For separating aerodynamic flows, it has been observed that Menter's SST model responds usually more appropriately to boundary layer separation than many other conventional eddy viscosity models. Indeed, by incorporating the Bradshaw assumption, the SST formulation has, to some extent, driven the resulting model to be of a *weakly* nonlinear type, with a more rational modeling for turbulent separating flows.

A rationale is highlighted here on the SST formulation for modelling boundary layer separation due to adverse pressure gradient. For comparison, the Wilcox standard $k-\omega$ model[5] is also taken in the analysis as an example of conventional eddy viscosity models. The production and dissipation/destruction terms in the k and ω equations are manipulated in the analysis. This is similar to the method by Peng and Davidson[8] in a previous analysis of a LRN $k-\omega$ model for predicting turbulent thermal flows with transition.

In order not to repeat the expressions of similar turbulent transport equations for both LRN and HRN forms, we present below the k and ω equations in LRN formulations, by which the HRN form can be readily recovered by setting a value of unity for all the empirical functions. The k and ω equations read, respectively,

$$\frac{\partial \rho k}{\partial t}+\frac{\partial(\rho u_j k)}{\partial x_j}=\tau_{ij}\frac{\partial u_i}{\partial x_j}-C_k f_k \rho k\omega+\frac{\partial}{\partial x_j}\left[(\mu+\frac{\mu_t}{\sigma_k})\frac{\partial k}{\partial x_j}\right] \tag{1}$$

$$\frac{\partial \rho \omega}{\partial t}+\frac{\partial(\rho u_j \omega)}{\partial x_j}=C_{\omega 1} f_\omega \frac{\omega}{k}\tau_{ij}\frac{\partial u_i}{\partial x_j}-C_{\omega 2}\rho\omega^2+\frac{\partial}{\partial x_j}\left[(\mu+\frac{\mu_t}{\sigma_\omega})\frac{\partial \omega}{\partial x_j}\right]+C_\omega\frac{\mu_t}{k}\frac{\partial k}{\partial x_j}\frac{\partial \omega}{\partial x_j} \tag{2}$$

The first three terms on the right-hand side in Eqs. (1) and (2) are subsequently the production term, the dissipation/destruction term and the diffusion term for k and ω, respectively. The last term in the ω equation is the cross diffusion term, $\mathcal{C}_{d\omega}$. The eddy viscosity, μ_t, in the $k-\omega$ model takes the form of

$$\mu_t=f_\mu\frac{\rho k}{\omega} \tag{3}$$

The turbulent stress tensor, τ_{ij}, appearing in the production terms in Eqs. (1) and (2), is generally formulated for linear eddy viscosity models as

$$\tau_{ij}=2\mu_t\left(S_{ij}-\frac{1}{3}\frac{\partial u_k}{\partial x_k}\delta_{ij}\right)-\frac{2}{3}\rho k\delta_{ij} \tag{4}$$

As mentioned, the transport equations presented above are for an LRN k-ω model, which will be used as the base model with the SST formulation. Similar forms of transport equations for k and ω are taken in Menter's SST model and Wilcox's standard $k-\omega$ model (STD $k-\omega$ model) by setting $f_\mu=f_k=f_\omega=1$. Moreover, the cross diffusion term in the ω-equation does not exist in the STD $k-\omega$ model, but appears for the SST model in the outer part of the wall layer (attained by means of a blending function[3]). Furthermore, it is noted that Menter's SST model takes a form for the production term of ω as $P_\omega=C_{\omega 1}\frac{\tau_{ij}}{\nu_t}\frac{\partial u_i}{\partial x_j}$. The details of the modelling formulation should be referred to Menter[3] for the SST model and to Wilcox[5] for the STD $k-\omega$ model.

As done by Wilcox[9] and by Peng and Davidson,[8] the *net* production for both k and ω is defined as the *net* gain per unit dissipation or destruction, namely, $N=(P-\Phi)/\Phi$, where P and Φ are the production term and the dissipation/destruction term, respectively, in the k or the ω equation. With the Wilcox STD $k-\omega$ model, the net productions for k and ω, namely, N_k^{STD} and N_ω^{STD}, take the following form, respectively,

$$N_k^{STD}=\frac{P_k}{\Phi_k}-1=\left(\frac{S}{\sqrt{C_k}\omega}\right)^2-1 \tag{5}$$

$$N_\omega^{STD}=\frac{P_\omega}{\Phi_\omega}-1=\left(\frac{S}{\sqrt{C_{\omega 2}/C_{\omega 1}}\omega}\right)^2-1 \tag{6}$$

With the SST assumption, the eddy viscosity in Menter's SST model is formulated by

$$\mu_t=\min\left(\frac{\rho k}{\omega},\frac{a_1\rho k}{F_2 S}\right) \tag{7}$$

where F_2 is an empirical function and $F_2 \in [0,1]$. For boundary layer separation, the second term in the parenthesis of Eq. (7) may become dominant over the first term which is the conventional eddy-viscosity formulation in a $k-\omega$ model. Taking approximately $F_2 \approx 1$ with Menter's SST model, the net productions, N_k^{SST} and N_ω^{SST}, for the k and the ω equation can be readily written as, respectively,

$$N_k^{SST} = \frac{P_k}{\Phi_k} - 1 = \frac{S}{\sqrt{C_k}\omega} - 1 \tag{8}$$

$$N_\omega^{SST} = \frac{P_\omega}{\Phi_\omega} - 1 = \left(\frac{S}{\sqrt{C_{\omega 2}/C_{\omega 1}}\omega}\right)^2 - 1 \tag{9}$$

Equations (6) and (9) suggest that the net production of ω in both models is the same, that is, $N_\omega^{STD} = N_\omega^{SST}$. For the turbulent kinetic energy, however, one has

$$N_k^{STD} = \left(\frac{S}{\sqrt{C_k}\omega} + 1\right) N_k^{SST} \tag{10}$$

Equation (10) indicates that, while the net production for the ω-equation holds the same for both the STD and SST models, the net production for the k-equation in the STD model is larger than in the SST model. As a consequence, the STD model may render a larger and faster growth of turbulent kinetic energy for flow separation, as compared to the SST model. The STD $k-\omega$ model may thus become more "diffusive" in modelling flow separation, usually leading to a suppressed separation bubble.

Prior to the presetnation of the SST concept in conjunction with an alternative $k-\omega$ model, it is emphasized here that the main purpose of the present work is to examine the modelling with and without the SST formulation incorporated into the based model, when applied to aerodynamic flows with local boundary layer separation. The focus in the computations of the test cases will thus be on an observation of the modelling performance in comparison with available experimental data. To set up reference solutions, Wilcox's STD model and Menter's SST model have also been invoked in the computations of the two test cases as presented in Section III.

B. The $k-\omega$ Model Incorporating SST Assumption

With the SST model for external aerodynamic flows, as indicated by Menter,[3] it is desired that the base model should be insensitive to the freestream turbulence intensity in order to accurately model the wall-layer flow features, particularly, in predictions of boundary layer flows with transition. Many variants of the $k-\varepsilon$ model may comply with this condition, but often possess a stiff wall boundary condition for ε. On the other hand, the advantage of the $k-\omega$ model is desirable in modelling wall turbulence, which gives rise of an analytical asymptotic solution for ω at the wall.[5,9] Accordingly, Menter's BSL model has been derived with an combination of a $k-\omega$ model in the near-wall region and a $k-\varepsilon$ model in the outer part of the wall boundary layer.

Being transformed from the $k-\varepsilon$ model and blended in the off-wall part, a cross diffusion term is present in the ω equation of the BSL model. As demonstrated by Menter,[3] the BSL model has been decoupled from the freestream dependency in the computation of a flat plate boundary layer with zero pressure gradient, whereas the Wilcox $k-\omega$ model may become significantly sensitive to different specifications of the freestream ω value. Obviously, this is largely due to the cross diffusion term present in the ω equation, which is an additional product when transforming the ε-equation into an ω-equation.[6,10,11] Along with different model coefficients, the addition of the cross diffusion term has driven the BSL $k-\omega$ model to behave differently from the original Wilcox $k-\omega$ model. In conjunction with the SST assumption, it is thus desirable that the selected base model should effectively rule out the freestream dependency in aerodynamic applications. For $k-\omega$ type models, this can be justified by the presence of the additional cross diffusion term in the ω equation with appropriate model constants.

In the present modelling formulation, we have chosen a modified $k-\omega$ model by Peng et al[6] as the base model. This $k-\omega$ model was originally developed for modelling internal flows characterized by separation and reattachment with local flow recirculation and mixing. The model was calibrated in its high-Reynolds number form,[7] and was developed further to a low-Reynolds number model by means of three empirical

damping functions.[6] Extension of the LRN $k-\omega$ model was also made for computations of turbulent heat transfer, where buoyancy imposes significant effects on turbulence production.[8]

Being taken as the baseline model in conjunction with the SST assumption, the formulation of the LRN model is briefly presented below, of which the details should be referred to Peng et al.[6] The turbulence transport equations for k and ω take the forms, respectively, as presented in Eqs. (1) and (2). The cross diffusion term, $\mathcal{C}_{d\omega}$ in the ω-equation holds overall in the near-wall layer and away from the wall.

The eddy viscosity, μ_t, in the LRN $k-\omega$ base model takes the form as in Eq. (3). The coefficients, f_μ, f_k and f_ω, appearing in the transport equations are empirical functions of the turbulent Reynolds number, $R_t = \mu_t/\mu$, being free of any wall parameters. These empirical functions take the following forms, respectively,

$$f_\mu = 0.025 + \left\{1 - \exp\left[-\left(\frac{R_t}{10}\right)^{3/4}\right]\right\}\left\{0.975 + \frac{0.001}{R_t}\exp\left[-\left(\frac{R_t}{200}\right)^2\right]\right\} \tag{11}$$

$$f_k = 1 - 0.722\exp\left[-\left(\frac{R_t}{10}\right)^4\right] \tag{12}$$

$$f_\omega = 1 + 4.3\exp\left[-\left(\frac{R_t}{1.5}\right)^{1/2}\right] \tag{13}$$

The model constants are $C_k = 0.09$, $C_{\omega 1} = 0.42$, $C_{\omega 1} = 0.075$, $C_\omega = 0.75$, $\sigma_k = 0.8$ and $\sigma_\omega = 1.35$. Note that, with the same model constants, the high-Reynolds number variant of the model is returned by setting $f_\mu = f_k = f_\omega \equiv 1$ (namely, for $R_t \to \infty$).[7]

The eddy viscosity defined as in Eq. (3) may over-predict the turbulent shear stress for a boundary layer with an adverse pressure gradient, where the production of k is much larger than its dissipation. As analyzed above using the net production, in other words, the eddy viscosity may be over-estimated and, consequently, pronouncing a too diffusive boundary layer. For transonic flows, furthermore, an over-predicted eddy viscosity will claim a delayed shock wave. This has been demonstrated in the simulation using the LRN $k-\omega$ model for the DLR-F6 configuration.[12]

With the present LRN model, the SST assumption is adopted in a similar way as by Menter[3] to reformulate the eddy viscosity, viz.

$$\mu_t = \frac{a_1 \rho k}{\max(a_1\omega/f_\mu, SF_2)} \tag{14}$$

where $a_1 = 0.31$ and F_2 is an empirical function. In the present work, we have taken the same formulation for F_2 from the SST model by Menter,[3] which takes the following form.

$$F_2 = \tanh\left\{\left[\max\left(\frac{2\sqrt{k}}{C_k\omega y}, \frac{500\mu}{\rho\omega y^2}\right)\right]^2\right\} \tag{15}$$

Note that, instead of using the magnitude of vorticity in Eq. (14), the magnitude of flow deformation, S, has been used, as in a later version of the Menter SST model.[4] By replacing Eq. (3) with Eq. (14), the SST assumption is incorporated in the present LRN $k-\omega$ model. This model is termed hereafter the *LRN SST* model. When setting a unity value to damping functions f_μ, f_k and f_ω, the LRN SST model is turned into a high-Reynolds number variant, which is termed hereafter the *HRN SST* model.

The addition of the cross diffusion term, $\mathcal{C}_{d\omega}$, in the ω equation does not modify the balance between the destruction term for ω, Φ_ω, and the viscous diffusion, $\mathcal{V}_d$, in the viscous sublayer. When integrated to the wall surface, that is, as the wall distance, y, approaching zero ($y \to 0$), the cross diffusion term, $\mathcal{C}_{d\omega}$ ($\propto y^0$) is much smaller than Φ_ω ($\propto y^{-4}$) and $\mathcal{V}_d$ ($\propto y^{-4}$). The balance of $\Phi_\omega = \mathcal{V}_d$ suggests that the asymptotic solution for ω holds, yielding $\omega \to 6\mu/(C_{\omega 2}\rho y^2)$ as $y \to 0$. In Menter's SST model, a constant value has been multiplied to this solution to mimic the wall value of ω, namely, at $y = 0$,

$$\omega = \alpha\frac{6\mu}{C_{\omega 2}\rho y_1^2} \tag{16}$$

where y_1 is the wall distance to the first node away from the wall surface, and $\alpha = 10$ for Menter's SST model. With the present LRN and HRN SST models, we have set $\alpha = 1$.

Moreover, it should be noted that the cross diffusion term in the present LRN model exists not only in the off-wall region but also when the model is integrated to the wall surface. With Menter's SST model, this term arises only in the outer part of the boundary layer by means of a blending function F_1.[3] The cross diffusion term may possess a large negative value in the vicinity of wall surface and changes its sign away from the wall after the peak of the near-wall turbulent kinetic energy. For computations of external aerodynamic flows, it has been observed occasionally that the change of the sign in $\mathcal{C}_{d\omega}$ may entail some numerical instabilities in the initial procedure when the solution is far from being converged, although this has not been observed in computations for incompressible internal flows with the LRN $k-\omega$ model. The large negative value of $\mathcal{C}_{d\omega}$ in the vicinity of wall surface is thus limited by the production term, $\mathcal{P}_\omega$, to avoid causing unphysical negative value of ω in the numerical procedure. Consequently, the following restriction on $\mathcal{C}_{d\omega}$ has been used.

$$\mathcal{C}_{d\omega} = -\min\left(\mathcal{P}_\omega, \left| C_\omega \frac{\mu_t}{k}\frac{\partial k}{\partial x_j}\frac{\partial \omega}{\partial x_j}\right|\right), \quad \text{if } \mathcal{C}_{d\omega} < 0 \tag{17}$$

III. Examination of Modelling

The modelling formulation is implemented in the EDGE CFD code, which is a node-based Euler/Navier-Stokes solver using the finite volume method. The general-purpose solver is applicable for aerodynamic flows ranging from subsonic to hypersonic regime on both structured and unstructured grids. To deal with turbulent flows, different modelling approaches are available in the solver, including conventional RANS (Reynolds-Averaged Navier-Stokes) two-equation models, algebraic and differential Reynolds stress models, as well as turbulence-resolving approaches, such as detached eddy simulation (DES), large eddy simulation (LES) and hybrid RANS-LES methods. In the present computations, the computation has been undertaken for steady flows. We have used the second-order central scheme to approximate the viscous flux and the convective flux in the Navier-Stokes equations and, for the convection term in the turbulent transport equations (namely, k and ω equations) a second-order upwind scheme with a TVD limiter is employed. The solution procedure is driven by a three-stage Runge-Kutta scheme with an implicit residual smoothing method. The convergence is accelerated with an agglomeration multigrid method by fusing finer control volumes onto the coarser grid level, which uses an injection operator for prolongation and its transpose for restriction. The details of the EDGE solver has been documented in Refs.[13,14]

To investigate the detailed modelling behavior, studies with fundamental flows would be desirable, for example, in simulations of turbulent boundary-layer flows with and without adverse pressure gradient. Nonetheless, the purpose in this work is to examine the modelling performance in aerodynamic applications with the SST concept incorporated into a $k-\omega$ base model. The resulting model has thus been directly applied to aerodynamic turbulent flows, for which conventional two-equation models may become awkward or inaccurate to resolve some inherent local flow features that are critical for overall aerodynamic performance. Two test cases have been computed in this work using both the LRN SST and HRN SST models, in comprison with other models, as well as with available experimental data. These include the flow around the RAE2822 airfoil and the flow around the DLR-F6 wing-body configuration.

A. Flow around RAE2822 Airfoil

The transonic flow around the RAE2822 airfoil is regarded as being a rather demanding test case in scrutinizing turbulence models. The flow is characterized by a shock-induced boundary layer separation arising at the location shortly after a half of chord on the suction side of the airfoil. The case computed here is denoted *Case 10* in some previous work.[15,16] The freestream flow has a Mach number of $M_\infty = 0.75$ and a chord-based Reynolds number of $Re = 6.2 \times 10^6$. The angle of attack is $\alpha = 2.8°$.[17] In all the computations, a turbulence instensity of 0.3% is specified in the freestream. A transitional region near the leading edge is specified over about 3% of the chord, c. The trailing edge of the airfoil is sharp and thus a C-type mesh has been used with about 1.3×10^5 nodes, see Figure 1 for a schematic view of the computational grid. The first node is placed at about $y_1 = 4 \times 10^{-6} c$ from the wall surface, which gives generally y_1^+ within the range of viscous sublayer. The far-field boundary of the computational domain has a distance of $20c$ from the airfoil.

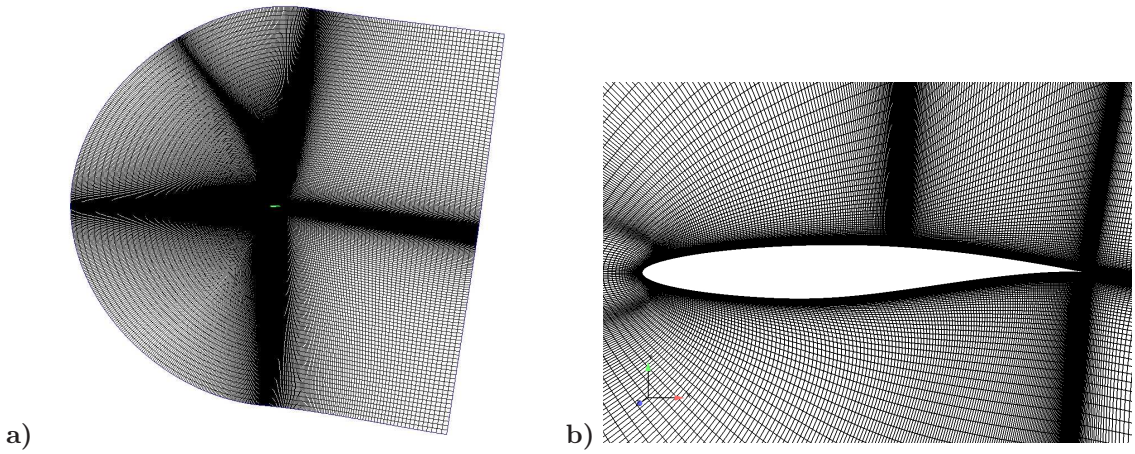

Figure 1. Schematic of the computational grid for the RAE2822 airfoil.

With this 2D airfoil test case, the main purpose is to examine the modelling of the shock-induced boundary layer separation in terms of the separation location, as well as the velocity and pressure distributions, in comparison with available experimental measurements. Along with Menter's SST model and Wilcox's $k-\omega$ model (STD $k-\omega$ model), other models invoked in the present computations include the LRN $k-\omega$ model by Peng et al.[6] (the PDH LRN $k-\omega$ model) and its high-Reynolds number form (the PDH HRN $k-\omega$ model), as well as their respective SST formulation, namely, the LRN SST model and the HRN SST model.

In Figure 2 a), the C_p countour is illustrated, from the computation by the LRN SST model. This figure provides a general view about the overall pressure distribution and the shock location. In Figure 2 b), the pressure distributions computed with various models are compared. It shows clearly that, without adopting the SST eddy-viscosity formulation, the STD $k-\omega$ model, the PDH LRN and HRN $k-\omega$ models have predicted a much delayed shock position as compared with the experimental measurement. By contrast, the LRN and HRN SST $k-\omega$ models, as well as Menter's SST model, have noticeably improved the predictions. Nonetheless, all the models have under-estimated C_p in the downstream after the separation bubble. This is due to the inaccurate modelling of the boundary layer recovery after the reattachment of the separation bubble, which is a weakness generally recognized for eddy-viscosity based models. The under-prediction in C_p after the separation is preserved even in predictions with advanced algebraic and differential Reynolds stress models.

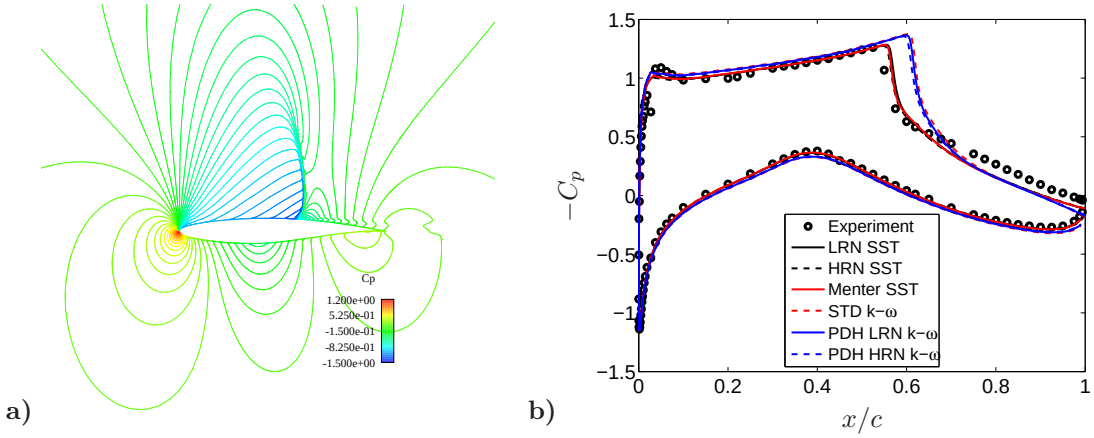

Figure 2. Pressure distributions around the airfoil. a) Overall C_p- contours by the LRN SST model; b) Comparison of pressure coefficient due to different models.

Apart from the C_p distribution presented in Figure 2, in order to highlight the predicted shock location by different models, Figure 3 presents further the contour of the Mach number, which is colored with the turbulence level in terms of the turbulent Reynolds number, $R_t = \mu_t/\mu$. The *measured* location at which

the shock is initiated, being indicated by the arrow in the figures, has been approximately estimated (at $x/c \approx 0.54$) from the measured pressure distribution. The improvement is obvious with the SST formulation for both the PDH HRN and LRN $k-\omega$ model, which is consistent to the pressure distribution over the shock wave presented in Fig. 2. As compared with the three models with SST formulation (i.e., the Menter SST model, the HRN and LRN SST models), the STD $k-\omega$ model, the original LRN and HRN $k-\omega$ models have estimated larger turbulent eddy viscosity (larger values of R_t) in the upstream boundary layer of the shock and in the downstream after the shock. These models have predicted a somewhat "thicker" shock wave than the SST models. Obviously, the SST formulation have made the model respond to the effect of adverse pressure gradient in a physically more appropriate way. Without the SST assumption incorporated, the models have over-predicted the eddy viscosity in the boundary layer entailing too a large turbulent diffusion. As a result, the predicted shock is delayed and becomes somewhat "diffusively" smeared.

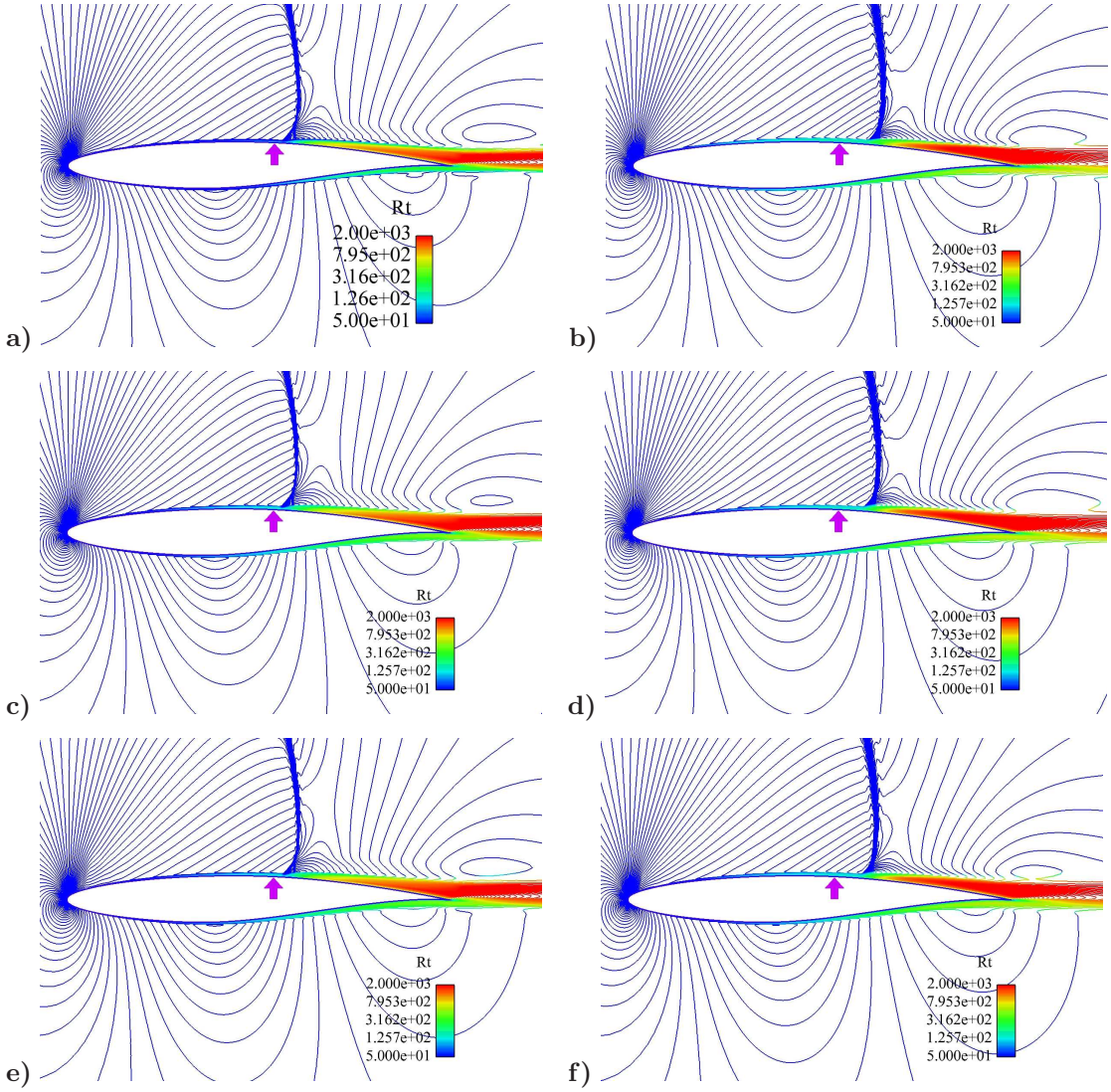

Figure 3. Mach number contour colored with the turbulent Reynolds number, $Rt = \mu_t/\mu$. The Arrow indicates approximately the location where the shock is initiated from experimental observation (at about $x/c = 0.54$). a) Menter's SST model; b) Wilcox STD $k-\omega$ model; c) HRN SST $k-\omega$ model; d) PDH HRN $k-\omega$ model; e) LRN SST $k-\omega$ model; f) PDH LRN $k-\omega$ model.

To make a quantitative examination, a comparison is further made in Figure 4 for the predicted streamwise velocity, u, at eight typical locations following the boundary layer over the suction side of the airfoil.

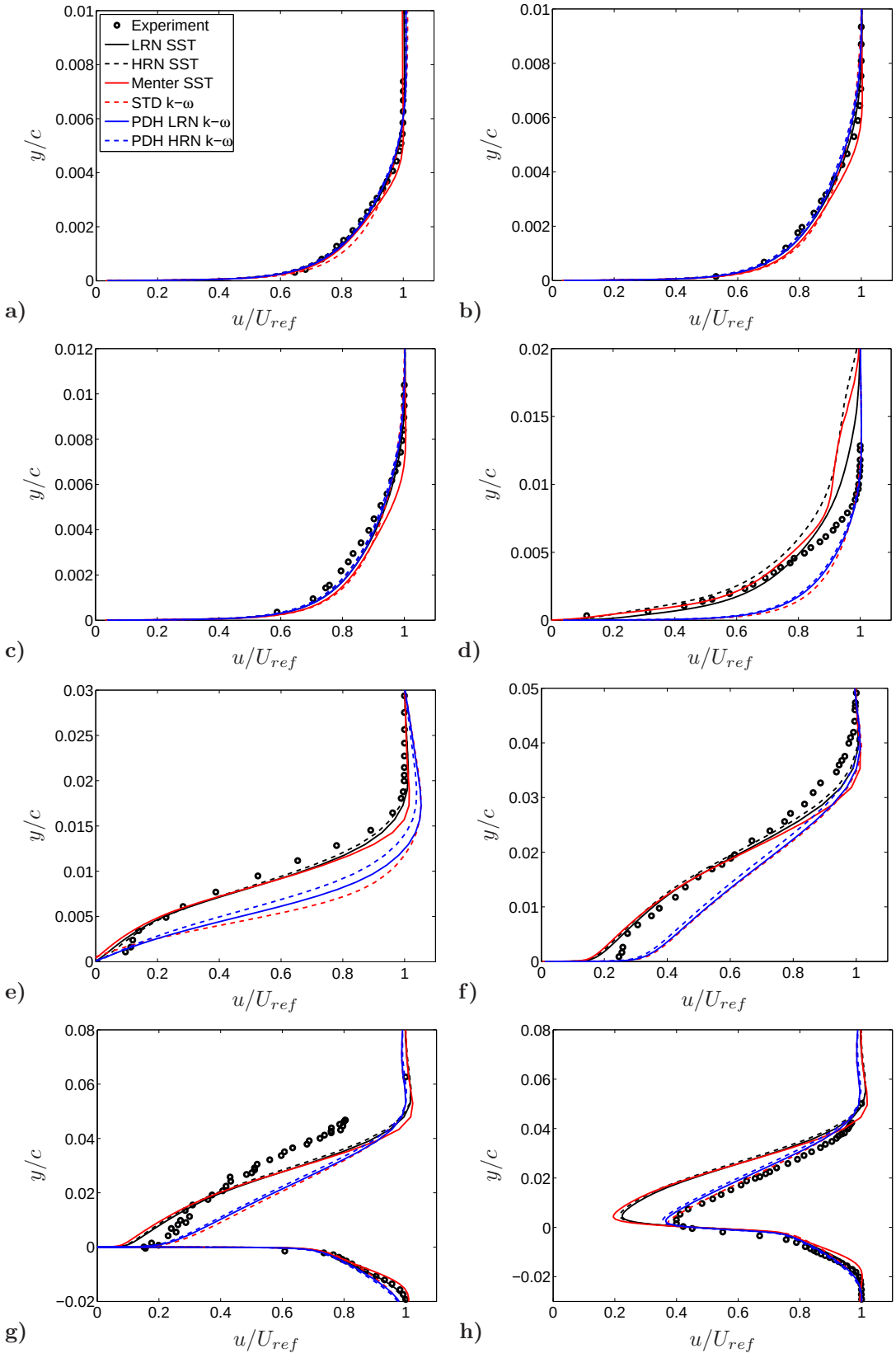

Figure 4. Comparison of streamwise velocity profiles over the suction side of the airfoil at locations: a) $x/c = 0.319$**; b)** $x/c = 0.404$**; c)** $x/c = 0.498$**; d)** $x/c = 0.574$**; e)** $x/c = 0.65$**; f)** $x/c = 0.90$**; g)** $x/c = 1.0$**; h)** $x/c = 1.025$**.**

Note that in Figure 4, $x/c = 0.574$ is a station shortly after the shock location measured by experiment. The station at $x/c = 1.0$ is located at the trailing edge, and $x/c = 1.025$ in the downstream trailing wake, as shown in Figures 4 g) and h), respectively. In the upstream attached boundary layer, namely, at $x/c = 0.319$, $x/c = 0.404$ and $x/c = 0.498$ in Fig. 4 a), b) and c), respectively, it is shown that the models have produced reasonable predictions for the streamwise velocity, but Menter's SST model has displayed a slight over-estimation in the outer part of the boundary layer and the STD $k-\omega$ in the near-wall part. Shortly after the measured shock location, at $x/c = 0.574$ (see Fig. 4 d)), the interaction between the shock and the boundary layer has hardly been reflected in the predictions by the models without using the SST formulation. This is due to the fact that these models have pronounced a delayed shock initiation (generally being predicted at about $x/c = 0.62$). The SST-based models are able to sensibly improve the prediction for the shock wave, as illustrated in both Figures 2 and 3. Consequently, at $x/c = 0.574$ in Fig. 4 d), the boundary layer computed by these models has responded to the effect of the shock, as indicated by the velocity profiles predicted at this location. In Fig. 4 d), it is also shown that, while the prediction near the wall is better than those obtained with the STD, LRN and HRN $k-\omega$ models, the predicted velocities with the three SST-based models are in discrepancies from the measured data in the outer part of the shear layer, with a marginally better prediction due to the LRN SST model. Further downstream after the shock, the three SST models are able to give generally better predictions, as illustrated at locations $x/c = 0.65$, $x/c = 0.90$ and $x/c = 1.0$ in Figures 4 e), f) and g), respectively. As mentioned, the STD, LRN and HRN $k-\omega$ models have predicted a delayed shock wave at about $x/c = 0.62$ (compared to the experimental value of $x/c \approx 0.54$). Without adopting the SST formulation, these models have modelled a nonphysically accelerating boundary-layer flow when approaching the *predicted* shock location. As shown, after $x/c = 0.574$ these models have generally over-estimated the velocity in the boundary layer. In the wake near the trailing edge (at $x/c = 1.025$), the velocity profiles predicted by the STD, LRN and HRN $k-\omega$ models collapse with the experimental data. This is however due to the over-predicted upstream velocities by these models, but not an inherent modelling accuracy.

B. Flow around DLR-F6 Wing-Body Configuration

The DLR-F6 wing-body (WB) configuration was adopted as a test case for two previous AIAA Drag Prediction Workshops (DPW), DPW II in 2003 and DPW III in 2006, respectively. Extensive computations have been made on this and modified configurations in our previous work,[12,18] with a number of turbulence models on different sets of grid at two different Reynolds numbers ($Re = 3\times10^6$ and $Re = 5\times10^6$). Previous studies have shown that the effect of Reynolds number is very small, but the prediction may become very sensitive when different sets of grids are employed.[18,19]

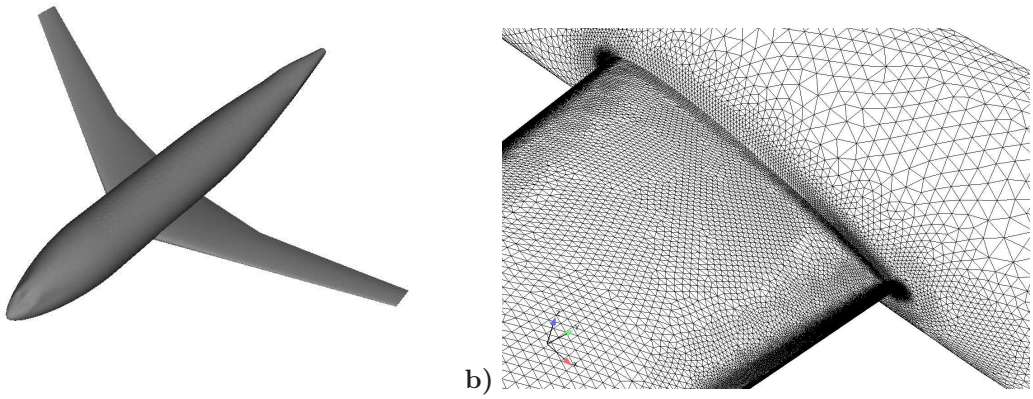

a) b)

Figure 5. a) Sketch of the DLR-F6 wing-body configuration; b) Local surface mesh (ANSYS grid) over the wing-fuselage junction.

For comparisons with available experimental data, the flow conditions in present computations have been specified with the freestream Mach number $M_\infty = 0.75$ and Reynolds number $Re = 3\times10^6$. The angle of attack is $\alpha = 1.23°$.

The main grid used in the computations is the intermediate grid generated by ANSYS for DPW III, which

is unstructured and contains about 8 million nodes. The sketch of the DLR-F6 wing-body configuration is illustrated in Figure 5 a). Also shown in Figure 5 b) is a local surface grid (by ANSYS) to highlight the grid resolution over the wing-fuselage junction region and the wing trailing edge.

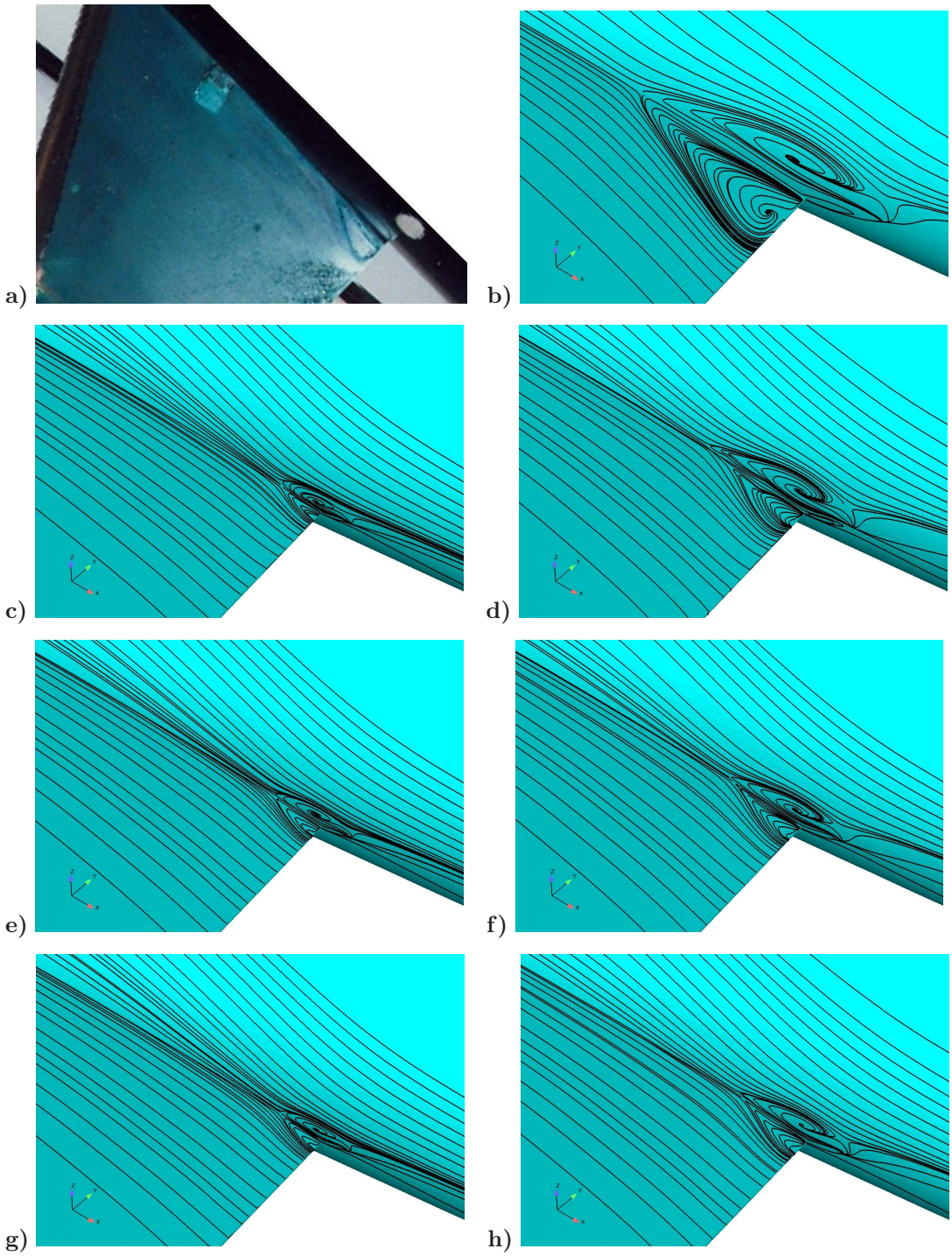

Figure 6. Separation bubble in the wing-body junction around the wing trailing edge. Prediction in b) is obtained with the DLR grid, and the ANSYS grid is used for predictions in c)-h). a) Experimental visualization by ONERA; b) LRN SST model with DLR grid; c) Wilcox STD $k-\omega$ model; d) Menter SST model; e) PDH HRN $k-\omega$ model; f) HRN SST model; g) PDH LRN $k-\omega$ model; h) LRN SST model.

As observed in the experimental visualization by ONERA, a separation bubble is disclosed in the wing-body junction around the wing trailing edge, as shown in Figure 6 a). Modelling of this separation bubble is related to the prediction of integrated forces and to the predicted pressure distributions on the inboard wing section. However, the prediction of this separation bubble is significantly sensitive to the grid used, as revealed in our previous studies,[18] where a grid-sensitivity study was conducted using two groups of subsequently refined grids from coarse, intermediate to fine resolution, respectively. With the same EARSM model, it was found that the group of ANSYS grids produce generally suppressed separation bubble, which is by contrast over-estimated on another group of grids generated by DLR for DPW III. Even with approximately similar node numbers, the DLR fine grid and the ANSYS intermediate grid have rendered very different pictures on the flow separation. Nonetheless, with the same group of grids, the prediction has shown a very small sensitivity to the grid refinement.[18]

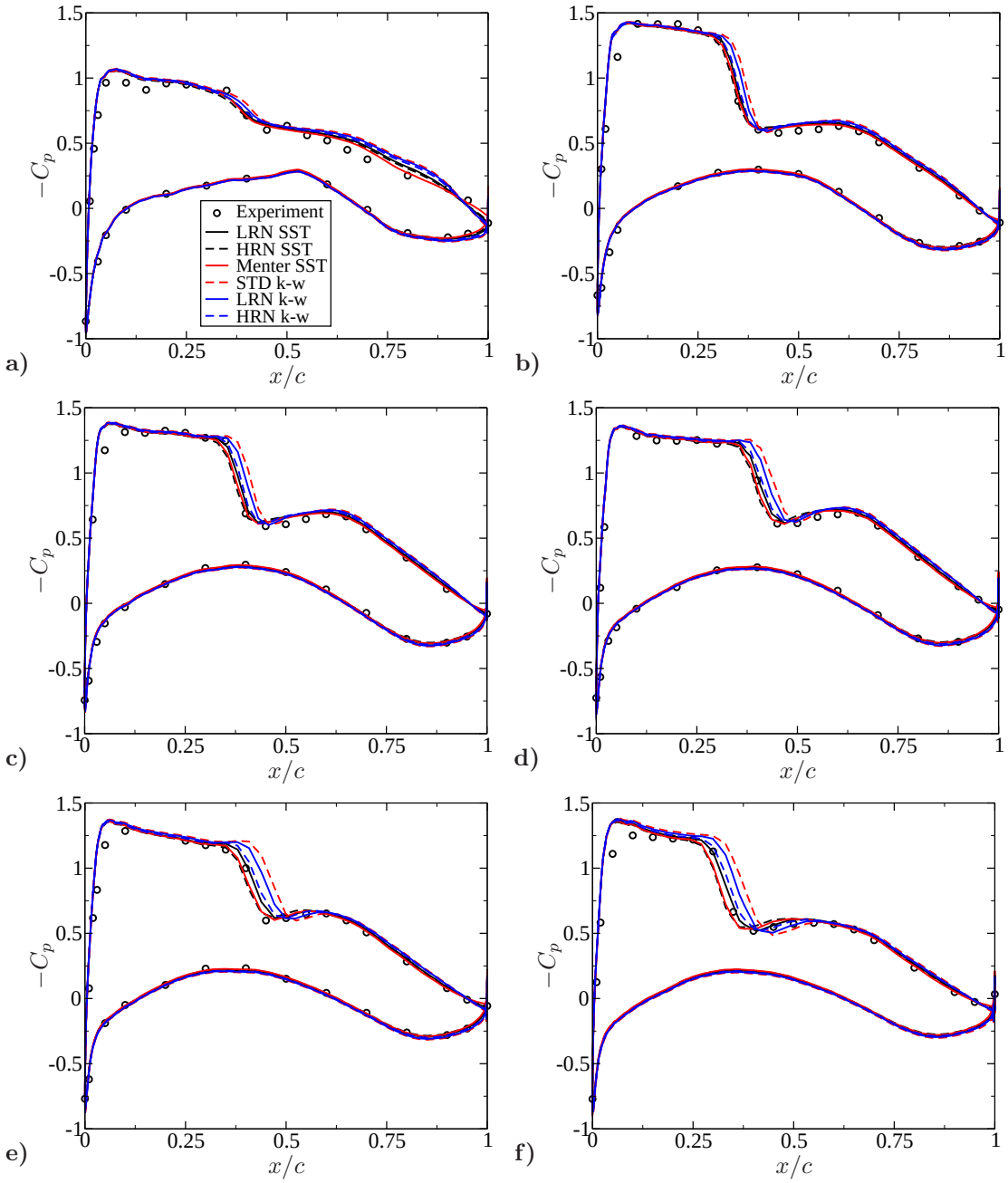

Figure 7. Pressure distributions in comparison with experimental data around various sections of the wing span at, respectively, a) $\eta = 0.150$; b) $\eta = 0.331$; c) $\eta = 0.377$; d) $\eta = 0.411$; e) $\eta = 0.514$; f) $\eta = 0.847$.

It is further noted here that, using the EARSM model,[20] the DLR grid gives better predictions for the integrated forces (drag, lift and pitching moment) than the ANSYS grid, while the shock location and the pressure distribution over the inboard wing section are better captured with the ANSYS grid.[18] As a test case in this work to quantitatively examine the SST modelling formulation, computations have been mainly carried out on the ANSYS intermediate grid. To give an impression on how the different sets of grids may affect the prediction for the separation bubble, a solution computed with the present LRN SST model on the DLR intermediate grid is also included, as shown in Figure 6 b). The details of these grids should be referred to Eliasson and Peng.[18]

The significant effect is highlighted by comparing Fig. 6 b) with Fig. 6 f) due to different grids, where the LRN SST model has been used respectively on the DLR and ANSYS grid. The DLR grid has produced a more extensive flow separation with a larger bubble size than the ANSYS grid. This is consistent with the previous investigation by Eliasson and Peng,[18] as mentioned above.

Figures 6 c)-h) have illustrated further a comparison of the separation bubbles on the ANSYS grid predicted with different models. These include the Wilcox STD $k-\omega$ model, the Menter SST model, the PDH HRN and LRN $k-\omega$ based models, and their respective SST variants. As shown, all the models have responded to the flow separation in the wing-body junction, but the separation bubble has been pronounced with very different extensions. Without the SST formulation, the STD $k-\omega$ model and the LRN and HRN $k-\omega$ models have produced a rather small separation bubble. As illustrated in Figures 6 d), f) and h), on the other hand, the SST formulation has enabled the models to claim a more extensive flow separation, giving a relatively large separation region, compared to the original base model. Although the under-estimation of the bubble size is preserved due mainly to the grid used, a direct incorporation of the SST formulation in the HRN and LRN $k-\omega$ models has shown rather promising performance in modelling of the boundary layer separation. The predicted separation by the LRN and HRN SST models is even more extensive than the prediction with an EARSM model on the same grid as displayed in Ref.[18]

The modelling has been further examined in a comparison of pressure distributions over different wing sections of the wing span. This is exhibited in Figure 7. Note that the location $\eta = 0.15$ is an inboard section close to the wing-body junction, and that η increases toward the wing tip. It is shown that the main difference lies generally in the prediction of the shock wave. At $\eta = 0.15$ (15% of the wing span), after the shock the C_p prediction is affected by the predicted separation bubble. As seen, the SST formulation has generally brought C_p closer to the experimental value than the models without using the SST assumption. In the predictions of the shock location, observable improvement has been attained with the SST formulation incorporated. Over the whole wing span, the STD $k-\omega$ model has predicted a delayed shock location, followed subsequently by the LRN and HRN $k-\omega$ models. The introduction of the SST formulation has obviously made the predictions improved over the original models. Both the HRN SST and the LRN SST models have produced C_p, as well as the shock location, in satisfactory agreement with the experimental data. The HRN SST model gives results very similar to these due to the Menter SST model.

IV. Conclusions

In conjunction with a previously proposed $k-\omega$ model with both its low-Reynolds and high-Reynolds number variants, the Shear Stress Transport (SST) concept is examined in aerodynamic flow computations. As the base model, the employed $k-\omega$ model includes a cross diffusion term in the ω equation, which is preserved in the wall layer as well as in regions away from the wall. Due to the inclusion of the cross diffusion term, the model is anticipated to be capable of diminishing the freestream sensitivity, and functioning similarly to Menter's BSL model in the outer part of the wall layer.

Based on an analysis of the *net* production, respectively, for the k and ω equations, the rationale of the SST formulation is highlighted. It is shown that in modelling boundary layer separation, the SST formulation induces a reduced net production of the turbulent kinetic energy and, consequently, contains its growth. The conventional eddy-viscosity formulation, by contrast, pronounces a relatively fast growth in the production of turbulence energy.

Incorporated into the alternative $k-\omega$ model, the SST formulation has invoked directly the model function, F_2, designed pragmatically in Menter's SST model. The resulting LRN and HRN SST models have been examined in computations for the RAE2822 airfoil flow and for the flow around the DLR-F6 aircraft configuration. Both flows are characterized by local boundary layer separation. Being scrutinized with available experimental data, the resulting LRN and HRN SST models are compared with the Menter

SST model, the standard $k-\omega$ model, as well as with the original LRN and HRN base models.

In line with the analysis on the net production, the predictions for both test cases have shown that the SST formulation is able to yield improved predictions over the original LRN and HRN base models, as well as over the STD $k-\omega$ model. This is particularly true in predictions for boundary layer separation over the airfoil/wing surface and for the shock location. Without incorporating the SST assumption, the model produces a too diffusive boundary layer, a suppressed flow separation and a delayed shock wave. With the SST formulation, the model becomes more *responsive* to the local flow properties, and entails a more extensive boundary-layer separation. The SST formulation helps to suppress the turbulent diffusion in regions with flow separation and with shock wave, rendering improved predictions in comparison with experimental observation.

References

[1]Vos, J. B., Rizzi, A., Darraq, D., and Hirschel, E. H., "Navier-Stokes solver in European aircraft design," *Progress Aerospace Sciences*, Vol. 38, 2002, pp. 601–697.

[2]Rumsey, C. L. and Ying, S. X., "Prediction of high lift: Review of present capability," *Progress in Aerospace Sciences*, Vol. 38, 2002, pp. 145–180.

[3]Menter, F., "Two-equation eddy-viscosity turbulence models for engineering applications," *AIAA J.*, Vol. 32, 1994, pp. 1598–1605.

[4]Menter, F. R., Kuntz, M., and Langtry, R., "Ten years of industrial experience with the SST turbulence model," *Turbulence, Heat and Mass Transfer 4*, Antalya, Turkey, October 12-17, 2003, 2003, pp. 73–86.

[5]Wilcox, D., "Reassessment of the scale-determining equation for advanced turbulence models," *AIAA J.*, Vol. 26, No. 11, 1988, pp. 1299–1310.

[6]Peng, S.-H., Davidson, L., and Holmberg, S., "A modified low-Reynolds-number $k-\omega$ model for recirculating flows," *ASME J. Fluids Engng*, Vol. 119, 1997, pp. 867–875.

[7]Peng, S.-H., Davidson, L., and Holmberg, S., "Performance of two-equation turbulence models for numerical simulation of ventilation flows," *5th Int. Conf. on Air Distributions in Rooms, ROOMVENT'96*, edited by S. Murakami, Vol. 2, Yokohama, Japan, 1996, pp. 153–160.

[8]Peng, S.-H. and Davidson, L., "Computation of turbulent buoyant flows in enclosures with low-Reynolds-number $k-\omega$ models," *Int. J. Heat and Fluid Flow*, Vol. 20, 1999, pp. 172–184.

[9]Wilcox, D., "Simulation of transition with a two-equation turbulence model," *AIAA J.*, Vol. 32, 1994, pp. 1192–1198.

[10]R., M. F., "Zonal two-equation $k-\omega$ turbulence model for aerodynamic flows," AIAA Paper 93-2906.

[11]Menter, F. R., "Eddy viscosity transport equations and their relation to the $k-\varepsilon$ model," *ASME J. of Fluids Engineering*, Vol. 119, 1997, pp. 876–884.

[12]Peng, S.-H. and Eliasson, P., "A comparison of turbulence models in prediction of flow around the DLR-F6 aircraft configuration," AIAA Paper 2004-4718, Providence, RI, 2004.

[13]Eliasson, P., "EDGE: A Navier-Stokes solver for unstructured grids," Scientific Report, FOI-R-0298-SE, FFA, Swedish Defence Research Agency, Stockholm, 2001.

[14]Eliasson, P., "EDGE: A Navier-Stokes solver for unstructured grids," *Proc. Finite Volumes for Complex Applications III*, 2002, pp. 527–534.

[15]Haase, W., Bradsma, F., Elsholz, E., Leschziner, M. A., and Schwamborn, D., *EUROVAL - An European Initialtive on Vaidation of CFD Codes*, Notes on Numerical Fluid Mechanics, Vol. 42, Vieweg Verlag, 1993.

[16]Haase, W., Chaput, E., Elsholz, E., Leschziner, M. A., and Mueller, U. R., *ECARP - European Computational Aerodynamics Research Project: Vaidation of CFD Codes and Assessment of Turbulence Models*, Notes on Numerical Fluid Mechanics, Vol. 58, Vieweg Verlag, 1997.

[17]Cook, P. H., McDononald, M., and Firmin, M. C. P., "Aerofoil 2822 - Pressure distributions, boundary layer and wake measurements," AGARD Advisort Report, AR 138, 1979.

[18]Eliasson, P. and Peng, S.-H., "Drag prediction for the DLR-F6 wing-body configuration using the Edge solver," AIAA Paper 2007-0897, Reno, NV, 2007.

[19]Vassberg, J., Tinoco, E. N., Mani, M., Brodersen, O. P., Eisfeld, B., Wahls, R. A., Morrison, J. H., Zickuhr, T., Laflin, K. R., and Mavriplis, D. J., "Summary of the Third AIAA CFD Drag Prediction Workshop," AIAA Paper 2007-260, Reno, NV, 2007.

[20]Wallin, S. and Johansson, A. V., "An explicit algebraic Reynolds stress model for compressible and incompressible turbulent flows," *Journal of Fluid Mechanics*, Vol. 403, 2000, pp. 89–132.